Electronic Supplementary Material (ESI) for Chemical Science.

Supporting Information for Spinterface chirality-induced spin selectivity effect in bio-molecules

Yonatan Dubi[*,†,‡]

†*Department of Chemistry, Ben Gurion University of the Negev, Be'er Sheva, Israel 8410501*

‡*Ilse Katz center for nanoscale science and technology, Ben Gurion University of the Negev, Be'er Sheva, Israel 8410501*

E-mail: jdubi@bgu.ac.il

S1. The "spinterface" mechanism for the CISS effect

For the sake of clarity and having the present paper self-contained, we briefly outline here the spinterface mechanism for the CISS effect. The reader can find a mre complete and detailed description in Ref. 1.

The starting point is the understanding that if the energy levels in the molecule (or in the electrode) are somehow spin-dependent (e.g. via Zeeman splitting), then naturally the energetics of the different spin-species would be different, leading directly to spin-selectivity (namely different transport properties for the different spins). An immediate possible cause for such Zeeman splitting is the simple fact that as current is passed through a helical molecule, a solenoid magnetic field is generated inside the molecule, which interacts with the electron spins. However, simple evaluation of the relevant field strengh (using the classical relation between field and current in a solenoid, $B_{sol} = \mu_0 n_t I$ where μ_0 is the permiability, n_t is the solenoid turn density and I the current) shows that the currents in molecular junctions are way too small (some 5-7 orders of magnitude) to generate the required Zeeman splitting that would lead to the spin-selectivity observed in experiments. Therefore, it is clear that a different mechanism is required to explain the observations.

The spinterface mechanism relies on several basic assumption. First, that the surface states of the metallic electrode are characterized by finite orbital angular momentum. This can be the angular momentum of the frontier orbitals of the atoms connected to the molecule (if the electrode states are localized and hence similar to the single-atom states), or they can be delocalized surface states. In either case, they are characterized by some finite orbital angular momentum $\vec{L}$.

Second, we assume that since angular momentum of charged particles carries with it a magnetic moment, then the surface states would also be affected by the solenoid field $\vec{B}_{sol}$. Since the generated field is in the z-direction, the energy associated with this interaction is $\mu\vec{B} \cdot \vec{L} = \alpha_0 \cos(\theta) I$, where α_0 is a constant (in units of energy/current) which takes into account the fundamental constants and the magnitude of the orbital angular momentum $|L|$. $\cos\theta$ is the tilt angle between the angular momentum and the molecular (z) axis.

However, this is not enough, because as pointed out above, the solenoid field is very small. Here comes the third assumption; if there is a spin-imbalance in the molecule (namely a difference in the density of spin-up and spin-down electrons, up and down referring to the directions parallel and anti-parallel to the molecular axis), then this generates an additional effective field (the spin-torque field) which is felt by the surface angular momentum. This assumption relies on the well-known consept of spin-transfer torque, namely the fact that as electrodes cross an interface the total angular momentum must be conserved. Therefore, an additional effective field of the form $B_{st} \alpha_1 \Delta n_s$ is felt by the surface angular momentm.

The combined action of these two fields, $_{eff} = B_{sol} + B_{st}$ works to stabilize the surface angular momentum at a finite tilt angle θ_M. The solenoid field is very small, but breaks the symmetry and determines the direction (parallel or anti-parallel to the molecular axis), while the spin-torque field B_{st} is much larger - but is spin-symmetric. Therefore, in the absence of a solenoid field (e.g. in a non-helical molecule) the average tilt angle will be $\theta_M = \pi/2$, meaning that *on average* the surface orbital magnetization vanishes, i.e.$\langle\vec{L}\rangle = 0$. Only due to the solenoid field a direction is fixed which allows for $\langle\vec{L}\rangle \neq 0$. This requires finite current, reflecting the non-equilibrium nature of te CISS effect.

The final assumption is that in the electrode there is finite spin-orbit coupling, of the form $\alpha_A \vec{L} \cdot \vec{S}$ (where $\vec{S}$ is the spin of the electrons in the electrode states). Therefore, if there is finite angular momentum, this leads to a difference in the energy of the different spin-species in the electrode, which translates to a spin-dependent chemical potential. This spin-dependent chemical potential leads to different transport properties of the different spin species, and hence to spin-filtering.

We point out that an essentially similar effect can be obtained if the interface interaction is not between the orbital angular momentum of the surface states and the combined solenoid-spin imbalance field in the molecule, but between the *spins* of the surface electrons and the effective solenoid-spin imbalance field in the molecule. The surface electron spins naturally interact with the solenoid field via a Hamiltonian term of the form $\vec{S} \cdot B_{sol}$. The interaction between the surface electron spins and the spin-imbalance in the molecule comes from spin-exchange couplingof the form $J\vec{S} \cdot \vec{s}$. Applying a (semi-classical) mean-field approximation to this kind of interaction would lead to exactly the same dynamics (and equations for the effective spin-dependent chemical potential) as described in Ref. 1.

S2. The CISS effect for small SOC in the electrodes

The theory presented in ref.[2] suggests that the CISS effect is due to the interplay between the spin-orbit coupling (SOC),α_A, in the electrodes in the spin-transfer torque between the electrode and the molecule, parametrized by an energy scale α_1. This description of the

CISS requires that there is some SOC in the electrode, but indeed it must not be very large - a small SOC coupling can be compensated by a larger α_1. This is important, since the CISS effect has been measured also with electrodes with much smaller SOC than those of Au (e.g. Ag, Al or Ni).

To demonstrate this, in Fig. 1(top panel) below we have repeated the calculation presented in Ref.[2] (single molecular level, weak coupling limit), namely the CISS polarization as a function of voltage, performing it for different values of SOC, $\alpha_A = 100, 31, 10, 3.1$ meV (all of them smaller than the SOC of AU, estimated at 0.5-1 eV). The top panel shows this calculation for $\alpha_1 = 10$meV, the same value used in Ref.[2] Even for these values, an appreciable polarization can be obtained ($\sim 5 - 8$ % at 0.5V).

However, if α_1 is increased to 100meV (bottom panel), substantial polarization can be achieved even for small SOC; the inset shows the polarization at V=0.5V as a function of α_A, showing polarization of $\sim$ 5% even for $\alpha_A = 3$ meV, two orders of magnitude smaller than the value for Au.

S3. Details for the theoretical calculation

Hamiltonian and Green's functions

The poly-CG double-strand DNA is described by a standard tight-binding single-particle Hamiltonian,

$$\begin{aligned}\mathcal{H}_{DNA} = &\sum_{j,\sigma}\sum_{s=1,2} \epsilon_{j,s}|js\sigma\rangle\langle js\sigma| \\ &+ \sum_{j,s,\sigma}\left(\alpha^s_{j,j+1}|ns\sigma\rangle\langle j+1, s\sigma| + h.c.\right) \\ &+ \sum_{j,\sigma}\left(\beta_j|j,1,\sigma\rangle\langle j,2,\sigma| + h.c.\right) \quad , \qquad (1)\end{aligned}$$

where j are the position index, $s = 1, 2$ are the two strands of the DNA and σ the carrier spin. $\epsilon_{j,s}$ are the onsite energies, $\alpha^s_{j,j+1}$ are the intra-strand couplings and β_j the inter-strand

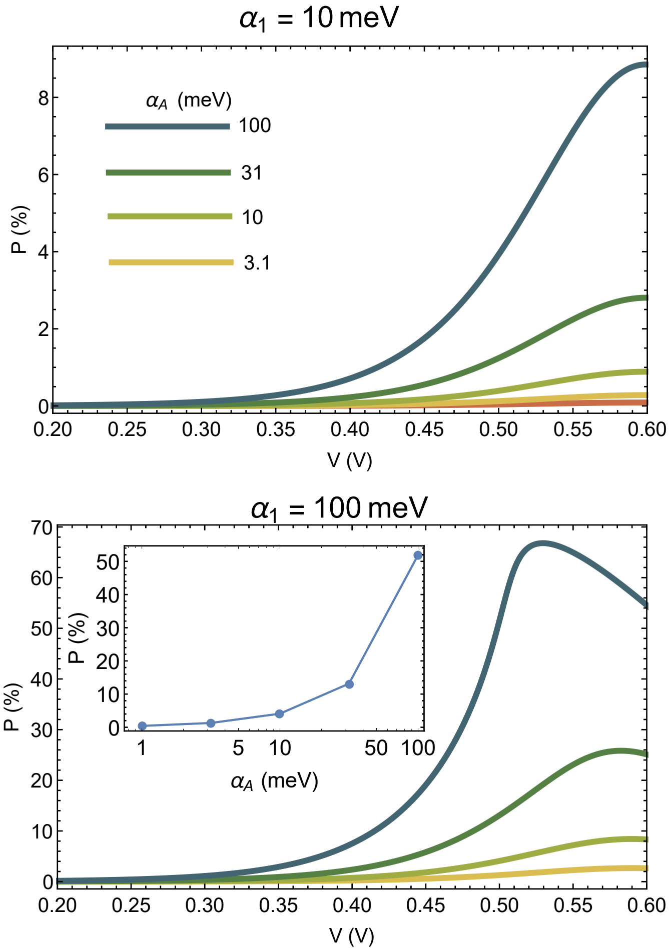

Figure 1: Top panel: Polarization P as a function of voltage for different values of the SOC, $\alpha_A = 100, 31, 10, 3.1$ meV, with $\alpha_1 = 10$ meV (all other parameters same as in Ref.[2] Bottom panel: same, for $\alpha_1 = 100$ meV. Inset: polarization at V=0.5V as a function of α_A.

couplings. For numerical values we use the parametrization of Refs.[3–6] The electrodes are described by simple (wide-band) self-energies[1,7]

$$\Sigma_L^{r,a} = \mp i\Gamma \sum_{j_L\sigma} |j_L\sigma\rangle\langle j_L\sigma| \ \ , \Sigma_{Rs}^{r,a} = \mp i\Gamma \sum_{j_R\sigma} |j_R\sigma\rangle\langle j_R\sigma|\delta_{\sigma s} \ \ . \tag{2}$$

where j_L and (j_R) are indices representing the contact sites between the molecule and the left (metallic) electrode and right (magnetic) electrodes. Note that the magnetic electrode only allows transfer of the majority spins (defined by the polarization of the electrode s).

To take into account $e-ph$ interactions, we resort to the self-consistent Green's function calculation,[8,9] which is applicable for soft phonons (i.e. with a broad spectral function). Within this approximation, the $e-ph$ coupling is encoded in a dephasing (retarded and advanced) self-energy $\Sigma_{deph}^{r,a}$, which is local in space, and defined by the self-consistent equation $\Sigma_{deph}^{r,a}(\omega) = \sum_{j,s} \gamma^2 [G^{r,a}(\omega)]_{js,js} |js\rangle\langle js|$, where γ is the $e-ph$ coupling strength, $[G^{r,a}(\omega)]_{js,js}\langle js| = G^{r,a}(\omega)|js\rangle$ and $G^{r,a}(\omega) = \left(\omega - \mathcal{H}_{DNA} + \Sigma_{deph}^{r,a}(\omega) + \Sigma_L^{r,a} + \Sigma_R^{r,a}\right)^{-1}$ are the retarded and advanced Green's functions (which are evaluated self-consistently along with the dephasing self-energy).

Currents and CISS effect

Once the Green's functions are evaluated self-consistently, the current, local density and the polarization are evaluated using the standard Landauer formula, $J_s = \frac{e}{h}\int d\varepsilon T_s(\varepsilon)\left(f_{L\sigma}(\varepsilon) - f_{R\sigma}(\varepsilon)\right)$, where $T_s(\varepsilon) = \mathrm{Tr}\left(\Sigma_L^r G_s^r \Sigma_{Rs}^a G^a\right)$. Similarly, the local electronic density (which is needed for the calculation of the spin-imbalance and the spin-transfer torque), given by $n_{\sigma s} = \int d\varepsilon \rho_{\sigma s}(\varepsilon)\left(\eta_L f_{L\sigma} + \eta_R f_{R\sigma}\right)$, where $\rho_{\sigma s}(\varepsilon) = -\frac{1}{\pi}\Im G_{\sigma s}^r(\varepsilon)$ is the electronic density of states, and $\eta_{L/Rs} = \frac{\Gamma_{L/Rs}}{\Gamma_L + \Gamma_{Rs}}$ weigh the coupling to the left and right electrodes.

The Fermi functions $f(\varepsilon) = \left(1 + \exp\left(\frac{\varepsilon-\mu}{k_B T}\right)\right)^{-1}$ depend on electrode (L,R) via a voltage bias $\pm V/2$, and on spin σ through the splitting of the chemical potential $\mu_\sigma = \mu + \sigma\alpha_A \cos(\theta_{M,\sigma})$, where α_A is the SOC in the metallic electrode, and $\theta_{M,\sigma}$ is the average angle between the surface magnetization in the metallic electrode and the molecular axis.

θ_M is determined self-consistently via the equation[1] $\cos(\theta_{M,\sigma}) = \mathcal{B}(\xi[\theta_{M,\sigma}])$, where $\mathcal{B}(x) = I_1(x)/I_0(x)$, where $I_n(x)$ are Bessel functions of the first kind, and $\xi[\theta_{M,\sigma}] = \frac{\alpha_0 J_\sigma[\theta_{M,\sigma}]+\alpha_1 \Delta S_\sigma[\theta_{M,\sigma}]}{k_B T}$. Here, $J_\sigma(V) = J_{\uparrow,\sigma}(V) + J_{\downarrow,\sigma}(V)$ is the total current (at a given magnetization direction σ of the magnetic electrode), and $\Delta S_\sigma = n_{\uparrow,\sigma}(V) - n_{\downarrow,\sigma}(V)$ is the spin-imbalance at the edge site of the molecular moiety. The currents and densities depend on $\theta_{M,\sigma}$ through the spin-dependent shift of the chemical potential, leading to a self-consistent solution. Once $\theta_{M,\sigma}$ is determined self-consistently, the spin-dependent currents are evaluated from the expression of the (spin-independent) current $J(V)$ through $J_\sigma(V) = J(V + \sigma\alpha_A \cos(\theta_{M,\sigma}(V))$.

S4. Length dependence of current and differential conductance

The currents and differential conductance of the molecular junction as a function of voltage is plotted in Fig. S1, for different values of chain length (ranging from 15 to 25 BPs, indicated by going from bright to dark, see legend). Changing the length of the chain shifts the conductance values, but does not alter the shape of the $J - V$ curves, thus leaving the differential conductance essentially indifferent to length. Since the polarization follows the differential conductance, it is also basically indiferent to molecular length.

S5. A rate-equation model for the experimental data

As pointed in the main text, in order to fit the experimental data with theory, one needs a model for transport through the junction, which can provide an expression for both the currents and the local densities. While in principle the model presented in Sec. 1 of this SI can be used, it requires fitting the exact DNA sequence, the γ parameter, and other unknowns of the system. Even then, it is likely that the model will not capture the currents correctly - because even using the DNA Hamiltonian with the parametrized energies is a

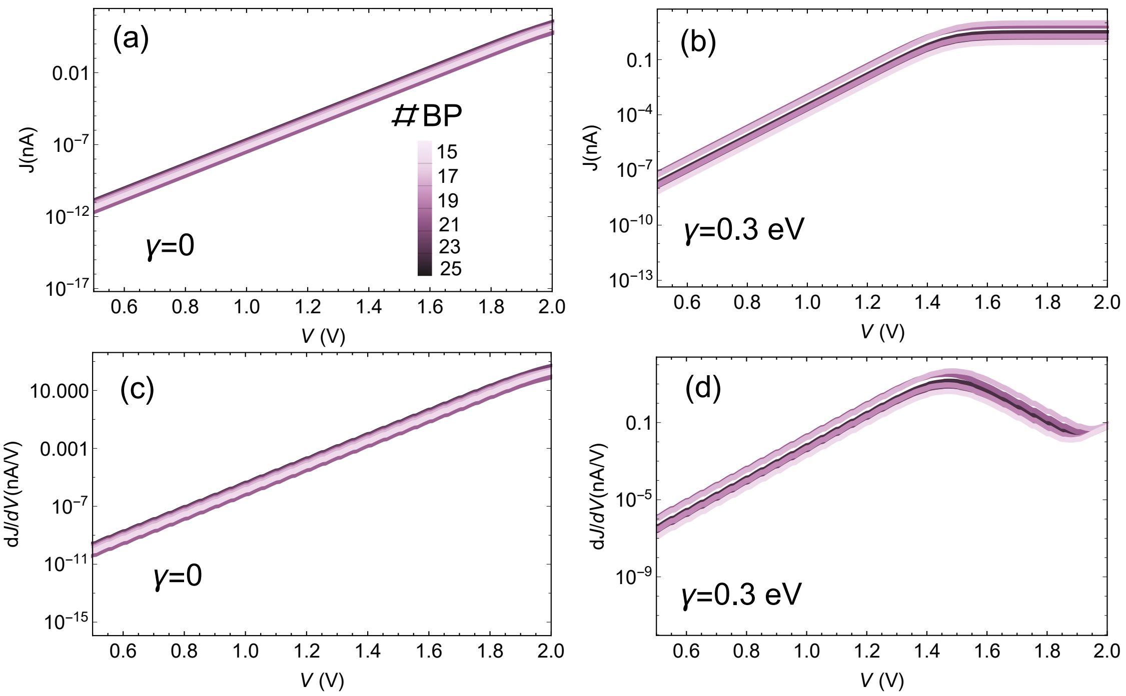

Figure 2: Currents (a-b) and differential conductance (c-d) as a function of voltage (lof scale), for difference molecular lengths (15-25 BPs, indicated by the legend) for $\gamma = 0$ ((a) and (c)) and $\gamma = 0.3$ eV ((b) and (d)).

huge over-simplification of the DNA chain.

in order to overcome this problem and still obtain simple model which can be used to analyze the experimental data, we note the following observation: although the model Hamiltonian presented in Sec. S1 above, including the $e-ph$ coupling parameter γ, describes a rather complicated system, its transport properties can actually be fitted by a very simple model of transport through only a few resonant energy levels. The reason is that although the level broadening Γ is quite large, transport is effectively done only via a few localized modes in the chain (a similar observation was done in,[10] where this fact can be seen through analyzing the transmission function), which are weakly coupled to the electrodes. This is the situation where the rate-equation formalism (see, e.g., Refs. 11 and 12) is applicable. Within the rate-equation model, transport through the system is described by a set of resonance energies ε_i, and transport through these levels is characterized by an electron transfer rate γ_i (in units of nA). The current through the junction is then simply given by[1,11]

$$J(V) = \sum_i \gamma_i \left(f_L(\varepsilon_i) - f_R(\varepsilon_i) \right) \quad , \tag{3}$$

where $f_{L/R} = \left(1 + \exp\left(\frac{\varepsilon_i \pm V/2}{k_B T}\right)\right)^{-1}$ are the left and right electrodes' Fermi distributions in the presence of voltage bias. Similarly, the density (and from it the spin-density imbalance, required for the CISS model), can be obtained using

$$n = \sum_i \frac{1}{2} \gamma_i \left(f_L(\varepsilon_i) + f_R(\varepsilon_i) \right) \quad . \tag{4}$$

In Fig. 3(a) we plot the $J - V$ curves for the 25BP chain, as extracted from the detailed formulation presented in Sec. S1 above (points), for $\gamma = 0$ (blue) and $\gamma = 0.3$ eV (black). The solid lines are fits to a rate-equation model. For the coherent case, we find that only one level is required to fully reconstruct the $J - V$ curve, while three levels are required for full reconstruction of the current for the incoherent ($\gamma = 0.3$eV) case. We point here that we can use the rate equation formalism to simultaneously fit both the currents and the densities (not shown), which requires typically an addition of 2-3 more levels.

In Fig. 3(b) we show the experimental bare $J - V$ curves, extracted from Ref. 13 (markers) and the experimental fits (solid lines). To obtain a good fit to the experimental data, the model required at least eight resonance levels (the fit parameters are shown in the table below). This demonstrates the complexity of the chosen molecules in Ref. 13, but allows us to fit the CISS data remarkably well. It is important to note that the theoretical description CISS effect and its fit to the data is completely orthogonal to the fits to the $J - V$ curves. Put simply, the transport parameters are obtained from the bare data (no CISS), and are kept the same for the fits shown in Fig. 4 of the main text.

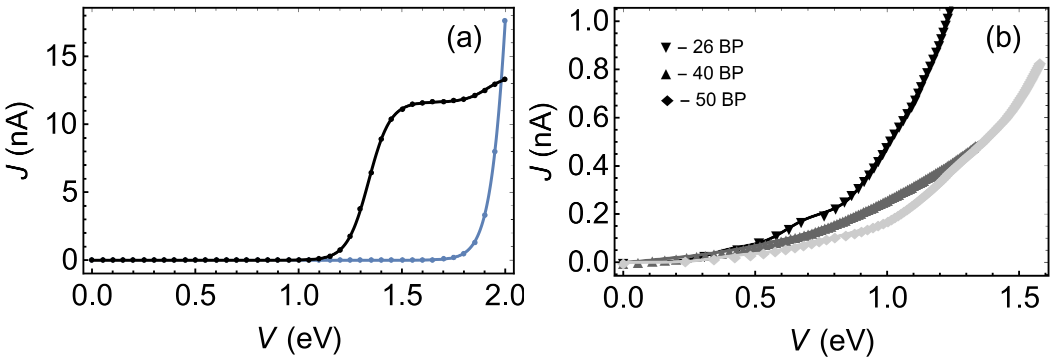

Figure 3: (a) $J - V$ curves obtained form the full theoretical description (points) and the rate-equation model (solid lines), for a 25BP chain with $\gamma = 0$ (blue) and $\gamma = 0.3$ eV (black). (b) Bare experimental $J - V$ curves, extracted from Xie et al.[13] (markers), and fits to the rate equation model (solid lines).

Table 1: Fit parameters for the data of Xuoti *et al.*.

26BPs	# 1	# 2	# 3	# 4	# 5	# 6	# 7	# 8
ε_i	0.758	0.175	0.526	0.606	0.31	0.81	0.42	0. 685
γ_i	0.21	0.034	0.12	0.179	0.058	0.33	0.048	0.12

40 BPs	# 1	# 2	# 3	# 4	# 5	# 6	# 7	# 8
ε_i	0.432	0.358	0.506	0.1666	0.578	0.262	0.66	0.062
γ_i	0.07	0.057	0.081	0.029	0.094	0.045	0.153	0.021

50 BPs	# 1	# 2	# 3	# 4	# 5	# 6	# 7	# 8
ε_i	0.606	0.526	0.424	0.319	0.685	0.758	0.175	0.812
γ_i	0.179	0.12	0.048	0.058	0.129	0.217	0.034	0.33

S6. Length-dependence: fit to experimental data of Mishra et al.[14]

Indeed, the methodology we presented in the previous SI section can be applied to various experimental data sets. We choose the data of Mishra et al. (Ref.[15] since it shows apparent length-dependent polarization, which seems to be at odds with the results shown in the manuscript. They are not.

To see this, we follow the same procedure as in the previous section. First, we use the average I-V curves (averaged over the magnetization directions of the magnetic electrodes) to obtain the transport parameters for different DNA lengths. Two notes are in order here. First, we were forced to use the average I-V curves (extracted by digitizing the figures in Ref.[15]), because no data for the control experiment with no electrode magnetization was supplied. Second, we chose here to use not the weak-coupling limit as for the data of Zuoti et al., but rather the strong coupling limit (see[1]), because this model seems to fit the experimental data much better. We find that even for the longest DNA chains, seperating the transmission function to transmission through 6-8 independent levels was enough to capture the I-V curves very well.

Once the transport parameters are obtained, we evaluate the currents for the two electrode magnetizations independently, and most importantly keeping the same parameters α_1 and α_A the same for all molecular lengths.

The results are shown in Fig. 4 below. We use for all lengths $\alpha_A = 0.82$ eV and $\alpha_1 = 4$meV. As can be seen, there is again remarkable agreement between the experimental data and the theory, thus corroborating our conclusion that the CISS mechanism is length-independent, and all the length-dependence arises from the length dependence of the transmission and spin polarization.

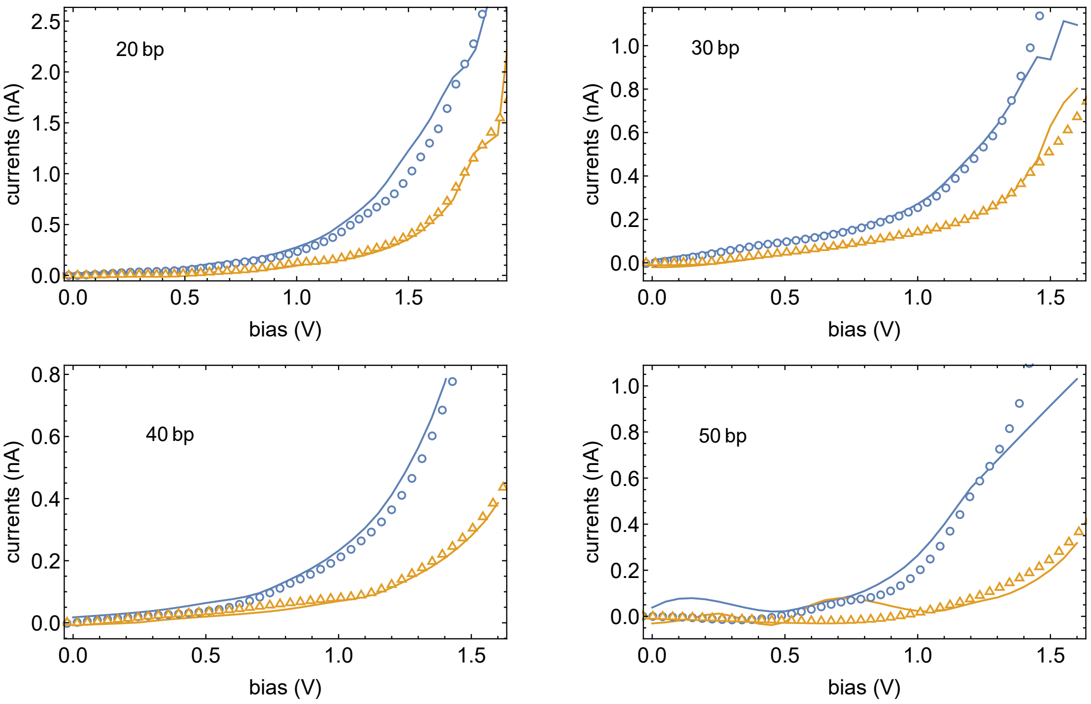

Figure 4: Currents as a function of voltage for two Ni electrode magnetization. Blue and orange represent the majority and minority polarization directions. Open markers are data extracted from Mishra et al.,[15] and solid lines are theoretical curves. For all DNA lengths we set $\alpha_A = 0.82$ eV and $\alpha_1 = 4$meV. The dicrepancy between theory and experiments at low voltages at 50BPs are due to the numerical extraction of the data.

References

(1) Alwan, S.; Dubi, Y. Spinterface Origin for the Chirality-Induced Spin-Selectivity Effect. *Journal of the American Chemical Society* **2021**, *143*, 14235–14241.

(2) Al-Bustami, H.; Koplovitz, G.; Primc, D.; Yochelis, S.; Capua, E.; Porath, D.; Naaman, R.; Paltiel, Y. Single nanoparticle magnetic spin memristor. *Small* **2018**, *14*, 1801249.

(3) Brisker-Klaiman, D.; Peskin, U. Coherent elastic transport contribution to currents through ordered DNA molecular junctions. *The Journal of Physical Chemistry C* **2010**, *114*, 19077–19082.

(4) Siriwong, K.; Voityuk, A. A.; Newton, M. D.; Rösch, N. Estimate of the reorganization energy for charge transfer in DNA. *The Journal of Physical Chemistry B* **2003**, *107*, 2595–2601.

(5) Voityuk, A. A.; Rösch, N.; Bixon, M.; Jortner, J. Electronic coupling for charge transfer and transport in DNA. *The Journal of Physical Chemistry B* **2000**, *104*, 9740–9745.

(6) Voityuk, A. A.; Jortner, J.; Bixon, M.; Rösch, N. Electronic coupling between Watson–Crick pairs for hole transfer and transport in desoxyribonucleic acid. *The Journal of Chemical Physics* **2001**, *114*, 5614–5620.

(7) Cuevas, J. C.; Scheer, E. *Molecular Electronics*; WORLD SCIENTIFIC, 2010.

(8) Dubi, Y. Transport through self-assembled monolayer molecular junctions: role of in-plane dephasing. *The Journal of Physical Chemistry C* **2014**, *118*, 21119–21127.

(9) Penazzi, G.; Pecchia, A.; Gupta, V.; Frauenheim, T. A self energy model of dephasing in molecular junctions. *The Journal of Physical Chemistry C* **2016**, *120*, 16383–16392.

(10) Guo, C.; Wang, K.; Zerah-Harush, E.; Hamill, J.; Wang, B.; Dubi, Y.; Xu, B. Molecular rectifier composed of DNA with high rectification ratio enabled by intercalation. *Nature chemistry* **2016**, *8*, 484–490.

(11) Xu, B.; Dubi, Y. Negative differential conductance in molecular junctions: an overview of experiment and theory. *Journal of Physics: Condensed Matter* **2015**, *27*, 263202.

(12) Mazal, Y.; Meir, Y.; Dubi, Y. Nonmonotonic thermoelectric currents and energy harvesting in interacting double quantum dots. *Phys. Rev. B* **2019**, *99*, 075433.

(13) Xie, Z.; Markus, T. Z.; Cohen, S. R.; Vager, Z.; Gutierrez, R.; Naaman, R. Spin Specific Electron Conduction through DNA Oligomers. *Nano Letters* **2011**, *11*, 4652–4655, PMID: 21961931.

(14) Mishra, S.; Pirbadian, S.; Mondal, A. K.; El-Naggar, M. Y.; Naaman, R. Spin-dependent electron transport through bacterial cell surface multiheme electron conduits. *Journal of the American Chemical Society* **2019**, *141*, 19198–19202.

(15) Mishra, S.; Mondal, A. K.; Pal, S.; Das, T. K.; Smolinsky, E. Z.; Siligardi, G.; Naaman, R. Length-dependent electron spin polarization in oligopeptides and DNA. *The Journal of Physical Chemistry C* **2020**, *124*, 10776–10782.